IEEE Open Journal of
Power Electronics

Received 1 April 2024; revised 8 May 2024 and 3 June 2024; accepted 17 June 2024. Date of publication 21 June 2024; date of current version 8 July 2024. The review of this article was arranged by Associate Editor Al-Thaddeus Avestruz.

Digital Object Identifier 10.1109/OJPEL.2024.3417177

Analysis and Cross-Coupling Elimination of Input-Series Output-Parallel (ISOP) Multi-Channel IPT System

PAN SUN [1], LEYU WANG [1], YAN LIANG [1], XUSHENG WU [1], AND QIJUN DENG [2]

[1]College of Electrical Engineering, Naval University of Engineering, Wuhan 430030, China
[2]School of Electrical Engineering and Automation,Wuhan University, Wuhan 430072, China

CORRESPONDING AUTHORS: LEYU WANG (e-mail: m22380811@nue.edu.cn); YAN LIANG (e-mail: 20100502@nue.edu.cn).

This work was supported in part by the National Natural Science Foundation of China under Grant 52007195 and Grant 52207182 and in part by the National Key Research and Development Program of China under Grant 2022YFC3102800.

ABSTRACT To meet the low-voltage and high-power demand of fast charging of electric vehicles, an ISOP multi-channel inductive power transfer (IPT) system based on LCC-S compensation network is analyzed in this paper. Firstly, the system's improvement of transmission capability is analyzed without considering the cross-coupling. After that, to clarify the cross-coupling impression, the equivalent impedance formula for the inverter output terminals of each channel is calculated. Then, combined with the harmonic characteristics of high order topology, the zero voltage switching (ZVS) condition of each channel is analyzed. Found out that the cross-coupling may lead to a decrease in the instantaneous current value when the inverter is turned on, thereby increasing the risk of losing the ZVS operating state. To eliminate the influence of cross-coupling, a parameter design method is proposed without additional devices and control. Finally, a 3-channel ISOP-IPT system prototype is built. The system achieves an energy transmission of 17.06 kW with an efficiency of 93.22%. Compared with single-channel systems, the power capacity is increased while keeping the input current level unchanged. After compensation, the system achieves equivalent decoupling in the case of cross-coupling, each channel works independently and maintains the input voltage balance.

INDEX TERMS Cross coupling, inductive power transfer (IPT), input-series output-parallel (ISOP), parameter compensation.

NOMENCLATURE

$G_1 \sim G_4$	Primary-side MOSFETs.
$D_1 \sim D_4$	Secondary-side rectifier diodes.
U_{single}, U_{in}	DC input voltage.
U_{o_single}, U_o	DC output voltage.
I_{single}, I_{in}	DC input current.
U_{in}, U_{ini}	Inverter output voltage.
i_l, i_{li}	Inverter output current.
i_p, i_{pi}	Primary-side coil current.
i_s, i_{si}	Secondary-side coil current.
R_{eq}, R_{eqi}	Secondary-side equivalent impedance
L, L_i	Primary-side compensation inductance.
C, C_i	Primary-side parallel compensation capacitor.
C_p, C_{pi}	Primary-side series compensation capacitor.
L_p, L_{pi}	Self-inductance of the transmitting coil.
L_s, L_{si}	Self-inductance of the receiving coil.
C_s, C_{si}	Secondary-side series compensation capacitor.
M, M_i	Mutual inductance between the transmitting and receiving coils.
M_a	Same-side mutual inductance.
M_b	Cross-side mutual inductance.
k_{Ui}	Voltage gain coefficient.
$K_i^{\pm}$	Proportional coefficient of input voltage between channels.
i_{bi}	The fundamental part of the inverter output current.
i_{hki}	The high-order harmonic part of the inverter output current.
C_{eqpi_in}	Primary-side series equivalent capacitance.
C_{eqsi_in}	Secondary-side series equivalent capacitance.

ω	The working angular frequency.
Z_{in}, Z_i	Equivalent impedance of inverter output.
Z_{pi}	Equivalent impedance of transmitting coil branch.

I. INTRODUCTION

Inductive power transfer (IPT) technology can realize non-contact power transmission. This non-contact characteristic makes it excellent for electrical isolation. Moreover, compared with the traditional wired transmission method, IPT technology has the advantages of safer, more reliable and easier construction, so it has a broader space for development and application. It has been widely used in electric vehicles [1], [2], implantable medical devices [3], underwater autonomous vehicles [4], [5] and smart electronic devices [6], etc.

Taking the electric vehicle application scenario as an example, the power transmission capacity of the IPT system needs to be increased. In [7], [8], three power levels of electric vehicle charging are given. Among them, Level 3 corresponds to the fast charging mode, the maximum power is 100 kW, and the voltage level is 204–600 V DC. Due to the limitations of rated voltage and current of power devices, single-channel IPT systems are difficult to meet the power requirements.

To solve the above problems, many scholars have studied the transmission power improvement of IPT system in low-voltage and high-power output scenarios. Existing methods include the following: cascade multi-level inverters [9], multi-inverter parallel [10], multi-coil transmission [11] and multi-channel system [12], [13], [14], [15].

In [9], [10], [11], the research ideas adopted are to improve the input power capacity of the transmitting side of the system, while there is no improvement on the receiving side. Because, the overall transmission power of the system is still limited by the rated voltage and current of the power device on the receiving side, and the rated output power is difficult to achieve a significant improvement. Moreover, considering the thermal stress of the current, the energy transmission of a single receiving channel is difficult to meet the long-term operation of the high-power system [16].

In the existing research on multi-channel system, four kinds of circuit structures are analyzed respectively: input-series output-series (ISOS) [12], input-parallel output-series (IPOS) [13], input-series output-parallel (ISOP) [14], input-parallel output-parallel (IPOP) [15]. Table 1 shows the circuit structure of the DC side and its application scenarios. For EVs fast charging, the ISOP circuit structure avoids the current loss caused by excessive bus current. And the output parallel structure is more suitable for low voltage, high current and high power requirements. Therefore, this paper focuses on the analysis of ISOP multi-channel system based on LCC-S compensation network.

In practical multi-channel systems, the system volume is often reduced by the close arrangement of coils, so it is inevitable to consider the influence of cross-inductance. The existing methods to eliminate cross-coupling include coupler design [15], [16], [17], control strategy [18], [19] and parameter design [20]. In [15], [17], the equivalent decoupling between couplers is realized through the structural design of couplers. In [18], an active reactance compensator is added to eliminate cross interference of multiple receiving channels. In [19], a combination of frequency control, duty cycle control and switching control capacitor (SCC) is used to achieve cross-coupled dynamic compensation of dual-load IPT systems. In [20], The optimal load reactance of the multi-receiver system is optimized to eliminate the cross-coupling effect. Some of these methods to eliminate cross-coupling fix the arrangement of coupling coils, and some only consider the decoupling of multi-coupling coils on the receiving side, which cannot be directly applied to ISOP-IPT system.

TABLE 1. DC Circuit Structure and Application Scenario of Multi-Channel System

Structure	Application scenario	Structure	Application scenario
ISOS [12]	High voltage input and output	ISOP [14]	High voltage input low voltage output
IPOS [13]	Low voltage input high voltage output	IPOP [15]	Low voltage input and output

Based on the analysis of the above problems, this paper focuses on improving the transmission power of IPT system and eliminating the cross-coupling effect of multi-channel system. The main research contents of this paper are as follows:

1) The power raising capability of ISOP-IPT system is analyzed. The theoretical equation for the equivalent impedance at the output of each inverter channel is derived when cross-coupling exists. Additionally, the variation trend of the fundamental impedance angle under different loads is analyzed.
2) Considering the harmonic characteristics of LCC-S high order topology, the influence of cross-coupling on the instantaneous current of each channel and the influence on the zero voltage switch (ZVS) are analyzed.
3) Without changing the circuit structure, the parameter design method is used to eliminate the inconsistency of inverter working state caused by the same-side mutual inductance, and to solve the input voltage imbalance caused by cross mutual inductance.

This paper is organized as follows: In Section II, the transmission characteristics of ISOP-IPT system without considering cross-coupling are analyzed. In Section III, the influence of cross-coupling on the operating state of each channel inverter is analyzed. In Section IV, the parameter design method is given to eliminate the influence of mutual inductance on the transmission characteristics of the system. Finally, in Section V, a three-channel ISOP-IPT experimental system is built to verify the correctness of the theoretical analysis. And the conclusion is drawn in Section VI.

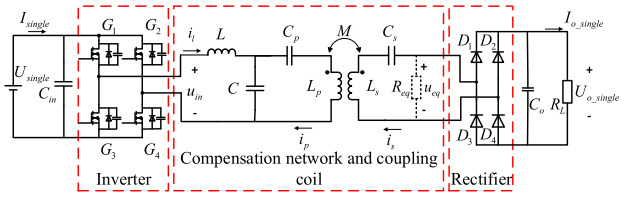

FIGURE 1. Single-channel IPT system based on LCC-S compensation network.

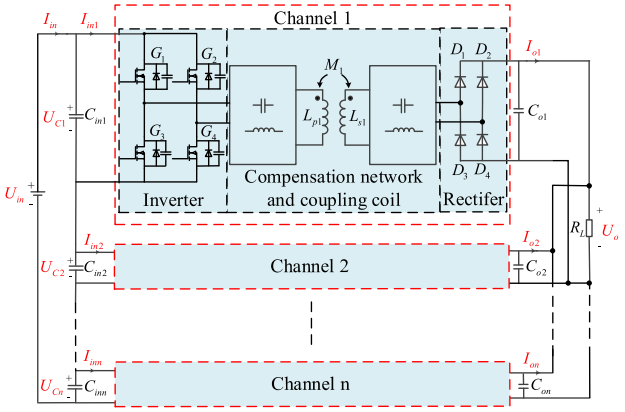

FIGURE 2. Circuit structure of multi-channel ISOP-IPT system based on LCC-S compensation network.

II. ANALYSIS OF TRANSMISSION CHARACTERISTICS OF ISOP-IPT SYSTEM WITHOUT CONSIDERING CROSS-INDUCTANCE

Compared with the four basic low-order compensation networks (S-S, S-P, P-S, P-P), the LCC-S high-order topology using multiple compensation elements has the advantages of higher design freedom, constant current of the original side coil, and the load independent output characteristics [21]. At the same time, the series compensation structure of the receiving side is simple and can reduce the number of compensation components, thus reducing the system volume. Therefore, the LCC-S compensation network is used as the basic structure in the subsequent analysis and research.

A. ANALYSIS OF SINGLE CHANNEL IPT SYSTEM

In order to analyze the circuit structure characteristics of multi-channel system, considering the simplified mode of traditional IPT system, the resistance of coupling-coil is ignored [22].

A typical single-channel IPT system based on LCC-S compensation network is shown in Fig. 1. It can be divided into three parts: full-bridge inverter, compensation network and coupling coil, and equivalent load. U_{single} is the DC input voltage, I_{single} is the DC input current, u_{in} is the inverter output voltage, i_l is the inverter output current, i_p and i_s are the transmitting coil and receiving coil currents, L, C and C_p constitute the transmitting side compensation network, and C_s is the receiving side compensation capacitor. L_p, L_s and M are coil self−inductance on the transmitting side and receiving side, and mutual inductance between coils, respectively. R_L is load resistance.

In order to improve the energy transmission efficiency of the system, the parameters of the compensation element and coil are usually designed to meet the following resonance conditions [23]:

$$\omega^2 = \frac{1}{LC} = \frac{1}{(L_p - L)C_p} = \frac{1}{L_s C_s} \tag{1}$$

where $\omega = 2\pi f$ is the circuit resonance angular frequency, f is the system operating frequency

Combined with the circuit shown in Fig. 1, when the compensation parameters meet (1), the voltage and current relationship of the system is as follows:

$$\begin{cases} Z_{in} = \dfrac{L^2 R_{eq}}{M^2} \\ I_p = \dfrac{2\sqrt{2}}{j\pi\omega L} U_{single} \\ I_s = \dfrac{\pi M U_{single}}{2\sqrt{2} L R_L} = \dfrac{\pi}{2\sqrt{2}} I_{o\_single} \\ U_{eq} = \dfrac{2\sqrt{2}M}{\pi L} U_{single} = \dfrac{2\sqrt{2}}{\pi} U_{o\_single} \end{cases} \tag{2}$$

The theoretical output power P_{out} of the system:

$$P_{out} = I_{o_{single}}^2 R_L = \frac{M^2 U_{single}^2}{L^2 R_L} \tag{3}$$

As can be seen from the (2), the equivalent impedance of the output end of the inverter is pure resistance, and the system can realize efficient transmission of energy. Moreover, the system has the characteristic of constant voltage output, and the output voltage is independent of the load.

B. CHARACTERISTIC ANALYSIS OF MULTI-CHANNEL ISOP-IPT SYSTEM

This part analyzes the input-series output-parallel (ISOP) inductive wireless power transmission system, and its circuit structure is shown in Fig. 2. In order to improve the stability of input and output voltage, parallel filter capacitors C_{ini} and C_{oi} are added at the front end of each channel inverter and the back end of rectifier. U_{Ci} is the input voltage of each channel inverter, I_{ini} is the input current of each inverter, U_{oi} is the rectifier output voltage, I_{oi} is the rectifier output current, and R_L is the load resistance.

According to the series and parallel circuit structure of the system, the voltage and current characteristics are as follows:

$$\begin{cases} I_{ini} = I_{inj} \\ U_{oi} = U_{oj} \\ U_{in} = \sum_{i=1}^{n} U_{Ci} \\ I_{in} = \sum_{i=1}^{n} I_{oi} \end{cases} \tag{4}$$

The AC steady-state circuit of each channel is shown in Fig. 3. Through analysis of (1) and (2) and the circuit shown in Fig. 2, the transmission characteristic equations of the circuit

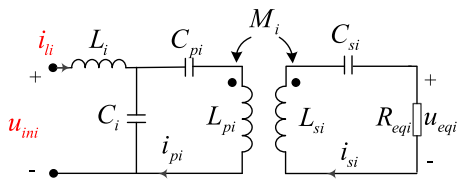

FIGURE 3. A channel steady-state circuit based on LCC-S compensation network in ISOP-IPT system.

can be obtained as follows:

$$\begin{cases} Z_{ini} = \dfrac{L_i^2 R_{eqi}}{M_i^2} = \dfrac{R_{eqi}}{k_{Ui}^2} \\ I_{pi} = \dfrac{2\sqrt{2}U_{Ci}}{j\pi\omega L_i} \\ I_{si} = \dfrac{\pi M_i U_{Ci}}{2\sqrt{2}L_i R_L} = \dfrac{\pi}{2\sqrt{2}} I_{oi} \\ U_{eqi} = \dfrac{2\sqrt{2}M_i U_{Ci}}{\pi L_i} = \dfrac{2\sqrt{2}}{\pi} k_{Ui} U_{Ci} = \dfrac{2\sqrt{2}}{\pi} U_o \end{cases} \tag{5}$$

where Z_{ini} is the equivalent impedance at the output of an inverter, I_{pi} and I_{si} is the RMS value of the transmitting and receiving coil current on each side. U_{eqi} is the RMS value of the input voltage of the rectifier, k_{Ui} is the voltage gain coefficient of each channel of the system.

Eq. (5) shows that, without considering cross mutual inductance, the equivalent impedance Z_{ini} at the output end of each channel inverter is pure resistance, and the system can realize efficient energy transmission. Meanwhile, the output voltage of each channel of the system is independent of load and has the characteristic of constant voltage output. According to the analysis of (4) and (5), the input-output relationship among channels of the whole system is as follows:

$$\begin{cases} \dfrac{U_{Ci}}{U_{Cj}} = \dfrac{I_{oi}}{I_{oj}} = \dfrac{L_i M_j}{L_j M_i} = \dfrac{k_{Uj}}{k_{Ui}} = \dfrac{R_{eqj}}{R_{eqi}} \\ I_o = \dfrac{1}{R_L}\sum_{i=1}^{n} \dfrac{M_i U_{Ci}}{L_i} \\ U_o = k_{Ui} U_{Ci} = k_{U1}\left[\sum_{j=1}^{n-1}\left(1 + \dfrac{k_{Uj}}{k_{U(j+1)}}\right)\right]^{-1} U_{in} \end{cases} \tag{6}$$

It can be seen from the above equation that the input voltage ratio and output current ratio of each channel of ISOP-IPT system based on LCC-S compensation network are related to series compensation inductance and transmission mutual inductance. And the input voltage ratio of each channel is inversely proportional to the voltage gain ratio. According to (5) and (6), when the compensation network parameters and mutual inductance of each channel are unchanged, the system has a constant-voltage output characteristic independent of load.

To compare the system power transmission capacity, assume that the series compensation inductor L_i and transmission mutual inductor M_i of each channel are equal. At this time, the multi-channel system output voltage is same as the single channel system output voltage ($U_{Ci} = U_{Cj} = U_{single}$). When the input voltage for each channel is the same as the input voltage for a single channel system, the total input voltage is n times that of a single channel system. And the output current and transmission power of the multi-channel system are increased the system's DC input current remains essentially the same as that of a single-channel system, effectively reducing bus losses.

TABLE 2. Simulation Parameters of Each Channel in ISOP System

Symbol	Value	Symbol	Value
L_i/μH	15	C_i/nF	233.7
L_{pi}/μH	95	C_{pi}/nF	43.824
L_{si}/μH	95	C_{si}/nF	36.904
M_1/μH	25	M_2/μH	20
M_3/μH	15	f/kHz	85
R_L/Ω	5	U_{in}/V	700

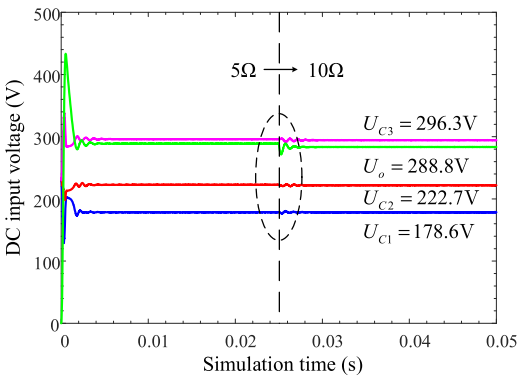

FIGURE 4. Simulation of DC input voltage in 3-channel ISOP-IPT system.

A 3-channel system simulation model was established to verify (6). Simulation parameters are shown in Table 2. The input voltage ratio and mutual inductance ratio of each channel in the system are as follows:

$$\frac{U_{C1}}{U_{C2}} = \frac{M_2}{M_1} = 0.8, \frac{U_{C2}}{U_{C3}} = \frac{M_3}{M_2} = 0.75$$

The simulation result is show in Fig. 4. The result shows that the relationship between the transmission characteristics of the system channels satisfies (6). At the simulation time of 0.025 s, the system load resistance changes from 5 Ω to 10 Ω. The input voltage of each channel and the output voltage of the system maintain the original voltage level after a small amplitude fluctuation. The system has constant voltage output characteristics.

From the above analysis, it can be seen that the input voltage and output current of the ISOP-IPT system are n times higher than that of the single-channel system without replacing the device with a higher power rating. The power is increased while maintaining a low system cost.

III ANALYSIS OF THE INFLUENCE OF CROSS-COUPLING ON THE TRANSMISSION CHARACTERISTICS

In Section II, the transmission characteristics of ISOP-IPT system without considering cross coupling have been analyzed, and can be used as a theoretical reference for system

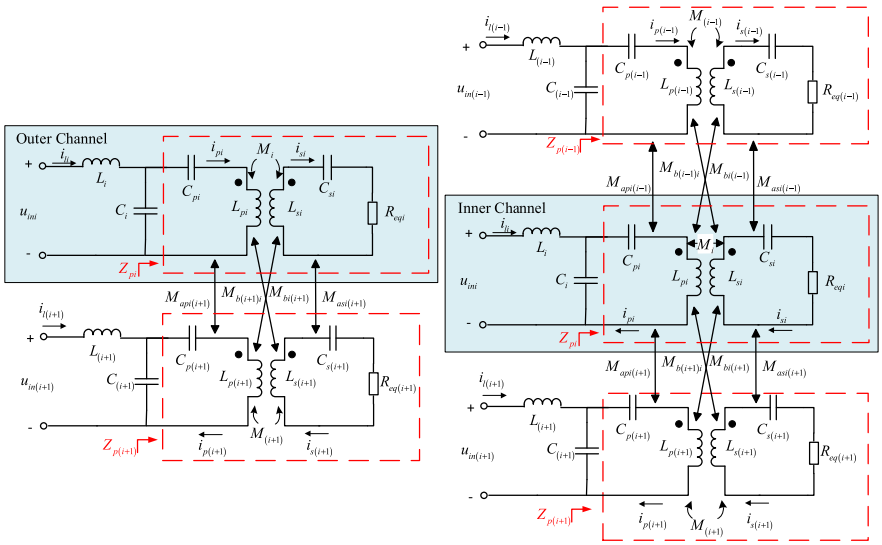

FIGURE 5. Multi-channel ISOP-IPT system steady-state circuit diagram.

parameter design. However, in the actual system design process, due to the limitation of system installation size and the requirement of high-power density, it is necessary to closely arrange each transmitting and receiving coil, which inevitably leads to cross coupling between the coils. The existence of cross coupling will change the original transmission characteristics of the system, making the output impedance angle and input voltage of the inverter in each channel of the system unbalanced. Therefore, it is very necessary to analyze the impact of cross coupling on the system and put forward corresponding compensation measures.

A. FUNDAMENTAL IMPEDANCE ANALYSIS OF INVERTER OUTPUT WITH CROSS-COUPLING CONSIDERED

Before analyzing the influence of cross-coupling on the transmission characteristics of each channel, the multi-channel ISOP-IPT system divides the channels into outer channels and inner channels based on the relative positions of the coils and the mutual effects between the channels, as shown in Fig. 5: 1) Outer channels: Channel 1 and Channel n are only affected by the cross-coupling of the adjacent channel. 2) Inner channels: All channels except Channel 1 and Channel n are simultaneously affected by the cross-coupling of the two adjacent channels. Since the distance between non-adjacent channels is much greater than the distance between two adjacent channels, only the cross-coupling effect between adjacent channels is considered in the analysis.

To simplify the analysis process, let's assume that the compensation parameters for each channel of the system, such as L_i, C_i, C_{pi}, C_{si} and the transmission mutual inductance M_i, same-side mutual inductance M_a and cross mutual inductance M_b, are all the same.

According to the circuit structure shown in Fig. 5, the voltage and current equations for the transmitting coil branch of the outer channel and inner channel can be obtained as follows:

$$\dot{\boldsymbol{U}}_i = \boldsymbol{A}_i\dot{\boldsymbol{I}}_i + \boldsymbol{B}_i\dot{\boldsymbol{I}}_{(i+1)} \cdots (i = 1) \tag{7.1}$$

$$\dot{\boldsymbol{U}}_i = \boldsymbol{A}_i\dot{\boldsymbol{I}}_i + \boldsymbol{B}_i\dot{\boldsymbol{I}}_{(i-1)} \cdots (i = n) \tag{7.2}$$

$$\dot{\boldsymbol{U}}_i = \boldsymbol{A}_i\dot{\boldsymbol{I}}_i + \boldsymbol{B}_i\left(\dot{\boldsymbol{I}}_{(i+1)} + \dot{\boldsymbol{I}}_{(i-1)}\right) \cdots (i \neq 1, n) \tag{7.3}$$

The matrix definitions in the equations are as follows:

$$\boldsymbol{A}_i = \begin{bmatrix} j\omega L_{pi} + \frac{1}{j\omega C_{pi}} & -j\omega M_i \\ -j\omega M_i & R_{eqi} \end{bmatrix}$$

$$\dot{\boldsymbol{U}}_i = \begin{bmatrix} \dot{U}_{pi} \\ 0 \end{bmatrix}, \dot{\boldsymbol{I}}_i = \begin{bmatrix} \dot{I}_{pi} \\ \dot{I}_{si} \end{bmatrix}, \boldsymbol{B} = \begin{bmatrix} j\omega M_a & -j\omega M_b \\ -j\omega M_b & j\omega M_a \end{bmatrix}$$

To simplify (7) further in order to obtain the impedance of the transmitting coil branch for each channel. Based on Kirchhoff's voltage law, the voltage and current equations for the series compensating inductor L_i and parallel compensating capacitor C_i in each channel circuit can be obtained as follows:

$$\dot{U}_{ini} = j\omega L_i\dot{I}_{li} + \frac{1}{j\omega C_i}\left(\dot{I}_{li} - \dot{I}_{pi}\right) \tag{8}$$

When the magnitude of L_i and C_i satisfies the resonance condition of the LCC-S compensating network, (8) can be simplified to express the relationship between the current in the transmitting coil branch and the output voltage of the inverter:

$$\dot{I}_{pi} = \frac{1}{j\omega L_i}\dot{U}_{ini} \tag{9}$$

Furthermore, based on the principle of power conservation, it can be understood that the input power of the inverter, the output power of the inverter, the input power of the rectifier, and the output power of the rectifier are equal:

$$U_{Ci}I_{ini} = \frac{U_{Coi}^2}{R_{Li}} \tag{10}$$

where R_{Li} is the equivalent impedance at the output terminals of each channel rectifier.

According to (4), (9), and (10) simultaneous calculation can be obtained.

$$K_i^{\pm} = \frac{R_{eqi}}{R_{eq(i\pm1)}} = \frac{\dot{I}_{s(i\pm1)}}{\dot{I}_{si}} = \frac{\dot{U}_{in(i\pm1)}}{\dot{U}_{ini}} = \frac{\dot{I}_{p(i\pm1)}L_{(i\pm1)}}{\dot{I}_{pi}L_i} \quad (11)$$

where $K_i^{\pm}$ is the proportional coefficient of equivalent loads among the rectifiers in different channels.

According to (11), the ratio of transmitting coil current and receiving coil current between each channel is inversely proportional to the equivalent load ratio of each channel rectifier.

Substitute (10) into (6) to simplify:

$$\dot{\boldsymbol{U}}_i = (\boldsymbol{A}_i + \boldsymbol{C}_1)\dot{\boldsymbol{I}}_i \cdots (i = 1) \quad (12.1)$$

$$\dot{\boldsymbol{U}}_i = (\boldsymbol{A}_i + \boldsymbol{C}_2)\dot{\boldsymbol{I}}_i \cdots (i = n) \quad (12.2)$$

$$\dot{\boldsymbol{U}}_i = (\boldsymbol{A}_i + \boldsymbol{C}_1 + \boldsymbol{C}_2)\dot{\boldsymbol{I}}_i \cdots (i \neq 1, n) \quad (12.3)$$

The matrix and coefficient in the (11) are as follows:

$$\boldsymbol{C}_1 = \boldsymbol{B}\begin{bmatrix} K_{Li}^{+} \\ K_i^{+} \end{bmatrix}, \boldsymbol{C}_2 = \boldsymbol{B}\begin{bmatrix} K_{Li}^{-} \\ K_i^{-} \end{bmatrix}, K_{Li}^{\pm} = K_i^{\pm}\frac{L_i}{L_{(i\pm1)}}$$

Based on (12), the equivalent impedance Z_{pi} of the transmitting coil branch at the transmitting side of each channel can be obtained, as shown in (13) shown at the bottom of this page, and then the equivalent impedance Z_{pi} can be divided into the resonant part of the compensation network Z_{lci} and the part affected by cross mutual inductance Z_{Mi} :

$$\begin{cases} Z_{lci} = j\omega L_{pi} + \frac{1}{j\omega C_{pi}} \\ Z_{pi} = Z_{lci} + Z_{Mi} \end{cases} \quad (14)$$

Combined with (1), (13) and (14), theoretical expression of the fundamental impedance Z_i at the output end of the inverter is calculated:

$$Z_i = \frac{L_i}{C_i Z_{Mi}} \quad (15)$$

The circuit simulation models of 3-channel and 5-channel ISOP-IPT systems were built, and the accuracy and applicability of the transmitter coil branch impedance equation of the above (15) were verified. As the actual coil cross-inductance measurement data are shown in Table 3 above, the cross-inductance is approximately 1/10 to 1/20 of the transmission mutual inductance. Therefore, in the verification process, the cross-inductance on the same side and cross-inductance on the different sides of each channel are set to be equal and 1/10 of the transmission mutual inductance. In the verification process, since the focus is on the accuracy of the equation, special consideration is not given to the parameters of the compensating components. The parameters of the compensating components for each channel are designed to be consistent, as shown in Table 4 above.

TABLE 3. Mutual Inductance Measurement Parameters of 3-Channel System

Symbol	Value	Symbol	Value
$M_1/\mu H$	33.9	$M_2/\mu H$	29.75
$M_3/\mu H$	32.68	$M_{ap12}/\mu H$	2.65
$M_{ap23}/\mu H$	2.45	$M_{as12}/\mu H$	2.9
$M_{as23}/\mu H$	2.42	$M_{b12}/\mu H$	1.6
$M_{b21}/\mu H$	1.35	$M_{b23}/\mu H$	1.95
$M_{b32}/\mu H$	1.78		

TABLE 4. Simulation Parameters of Each Channel in ISOP System

Symbol	Value	Symbol	Value
$L_i/\mu H$	15	C_i/nF	233.7
$L_{pi}/\mu H$	95	C_{pi}/nF	43.824
$L_{si}/\mu H$	95	C_{si}/nF	36.904
$M_i/\mu H$	20	$M_a/\mu H$	2
$M_b/\mu H$	2	f/kHz	85
R_L/Ω	5~20	U_{in}/V	700

In calculations where high parameter accuracy is required, such as during parameter identification [24], the non-linear characteristics of the rectifier make it inappropriate to directly equate the rectifier and load resistance to a purely resistive load. Considering that the equivalent impedance of the rectifier on the receiving side contains inductive components, the influence of the weak inductive equivalent impedance of the rectifier is not focused on in the process of equation verification. Therefore, in order to mitigate the impact caused by the inductive components of the equivalent impedance of the rectifier, the equivalent impedance value used in the calculation process should be based on the AC fundamental impedance values of the rectifier's input voltage and current obtained from simulations.

The final comparison between the mode and phase angle of the fundamental impedance at the output of each channel's inverter, and the simulated values is shown in Fig. 6: The simulation results of equivalent impedance mode and

$$\begin{cases} Z_{Mi} = j\omega M_a K_{Li}^{\pm} + \frac{\omega^2(M_i+M_bK_{Li}^{\pm})(M_i+M_bK_i^{\pm})}{R_{eqi}+j\omega M_a K_i^{\pm}} \cdots (i = 1, n) \\ Z_{Mi} = j\omega M_a\left(K_{Li}^{+} + K_{Li}^{-}\right) + \frac{\omega^2[M_i+M_b(K_{Li}^{+}+K_{Li}^{-})][M_i+M_b(K_i^{+}+K_i^{-})]}{R_{eqi}+j\omega M_a(K_i^{+}+K_i^{-})} \cdots (i \neq 1, n) \\ Z_{pi} = j\omega L_{pi} + \frac{1}{j\omega C_{pi}} + Z_{Mi} \end{cases} \quad (13)$$

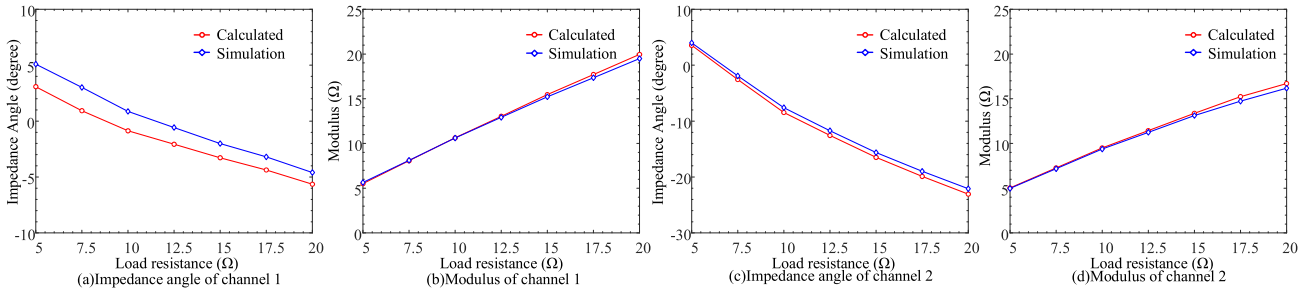

FIGURE 6. Equivalent impedance for a 3-channel ISOP-IPT system considering cross mutual inductance.

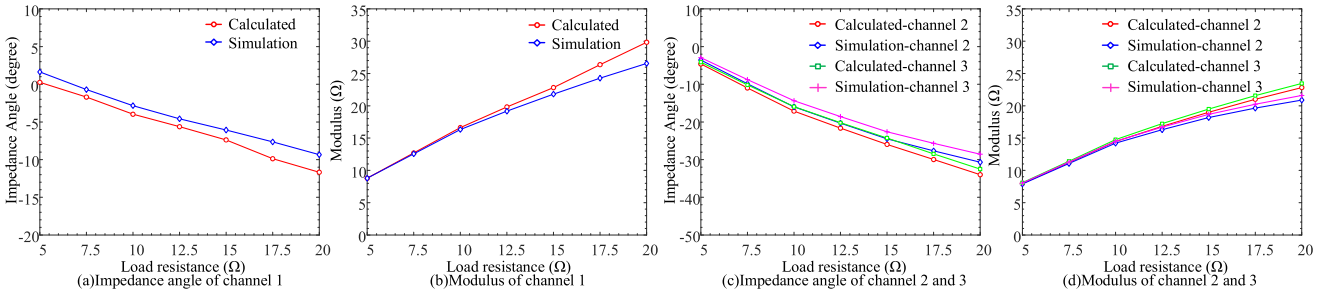

FIGURE 7. Equivalent impedance for a 5-channel ISOP-IPT system considering cross mutual inductance.

impedance angle of channel 1 and channel 2 inverters in 3 channel ISOP-IPT system show that the calculation error of impedance angle is less than 2%, and the calculation error of impedance mode is less than 5%. At the same time, in order to verify the multi-channel applicability of the equation, a 5 channel ISOP-IPT system was simulated and verified, and the results were shown in Fig. 7. Considering the symmetry of the whole system, only the comparison results of channels 1, 2 and 3 are given here. The calculated results of the equivalent impedance mode and phase angle at the output of each channel's inverters are generally consistent with the simulation results, exhibiting similar trends. Therefore, it can be considered that (15) can reflect the influence of cross coupling on the branch impedance of the transmitting coil at the transmitting side.

Moreover, according to the simulation results in Figs. 6 and 7, when cross coupling exists, the fundamental impedance angle of the inverter output end of each channel in the 3-channel ISOP-IPT system decreases with the increase of load resistance, and the change amplitude of the inner channel is greater than that of the outer channel. This effect will lead to the phase difference of the fundamental current at the output end of the inverter, which will affect the consistency of the working state of the inverter in each channel. In the subsequent analysis, the mutual inductance components that affect the fundamental impedance angles are mainly analyzed and eliminated, so that the fundamental impedance angles of each channel in the presence of cross coupling are the same, and the inconsistency between the working states of the system channels is eliminated.

B. THE ANALYSIS OF THE WORKING STATE OF EACH CHANNEL INVERTER OUTPUT CONSIDERING THE HIGHER HARMONICS

According to the research in [25], the presence of cross coupling inductance can affect the equivalent impedance at the output of each channel's inverter, leading to a phase difference between the inverter's output voltage and current. This increases the risk of each channel's inverter losing its ZVS operating state. Not only that, in the actual system analysis process, because the LCC-S high-order compensation network is used in the circuit, the higher harmonics are included in the partial circuit branches of the transmitting side of the system, which will also affect the working condition of the switching device. Therefore, when analyzing the influence of cross coupling on multi-channel ISOP-IPT system, the influence of higher harmonics should also be analyzed.

Based on the [26], when considering higher-order harmonics in the LCC-S compensation network, it is possible to approximate the effect of higher-order harmonics by considering only the series-compensated inductive and shunt-compensated capacitive circuit loops. During calculations, the circuit consisting of the series compensation inductors L_i and the parallel compensation capacitors C_i is equivalently represented as a circuit containing harmonic components, as shown in Fig. 8.

When considering higher harmonics, the instantaneous output current of each channel inverter at switching time is analyzed to reflect the working state of each channel inverter. At the same time, the variation trend between load resistance and current instantaneous value is analyzed.

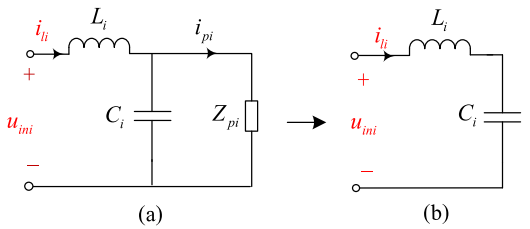

FIGURE 8. A simplified circuit containing higher harmonics on the transmitting side.

First of all, the Fourier expansion of the output voltage of the inverter in each channel of the system is as follows:

$$u_{ini\_k}(t) = \sum_{k=1}^{n} \frac{4U_{Ci}}{k\pi} \sin(k\omega t) \tag{16}$$

Then, according to the circuit containing harmonic parts in Fig. 8, the circuit equation of higher harmonics is listed as follows:

$$\dot{U}_{ini\_k} = j\left(k\omega L_i - \frac{1}{k\omega C_i}\right)\dot{I}_{li\_k} \tag{17}$$

Each channel series compensating inductor L_i and parallel compensating capacitor C_i satisfy the resonant condition of the fundamental frequency of (1). By substituting the resonant condition into (17), the circuit equivalent impedance Z_{hki} of the output higher harmonics of each channel inverter can be obtained as follows:

$$Z_{hki} = \frac{k^2 - 1}{k} j\omega L_i \tag{18}$$

where k is the harmonic number

According to (15) and (18), under the condition of fixed parameters for the circuit compensation elements, the impedance Z_i is influenced by changes in the load and cross-coupling inductance. The impedance Z_{hki} is purely inductive and only depends on the size of the series-compensated inductor, without being affected by the load resistance.

Then, according to Ohm's law, the time domain expression of i_{hki} is calculated as follows:

$$i_{hki}(t) = \frac{|\dot{U}_{ini\_k}|}{|Z_{hki}|} \sin(k\omega t - \alpha_{hki}) \tag{19}$$

where $\alpha_{hki} = \frac{\pi}{2}$ is the impedance angle of the higher order harmonic circuit.

According to (15), the time domain expression of the output fundamental current i_{bi} of each channel inverter is obtained as follows:

$$i_{bi}(t) = \frac{|\dot{U}_{ini\_1}|}{|Z_i|} \sin(\omega t - \alpha_i) \tag{20}$$

where $\alpha_i = \tan^{-1}\frac{\mathrm{Im}(Z_i)}{\mathrm{Re}(Z_i)}$ is the fundamental wave impedance angle.

Combined with (19) and (20), the time domain expression of the total output current i_{li} of the inverter can be obtained according to the superposition theorem:

$$i_{li}(t) = i_{bi}(t) + \sum_{k=1}^{n} i_{hki}(t) \tag{21}$$

According to the above calculation process and the equation in Section III-A, when higher-order harmonics and cross-coupling inductance are present, they primarily affect the equivalent impedance of each channel in an ISOP-IPT system. Consequently, this can impact the magnitude of the instantaneous current values at the moment of inverter turn-on. Meanwhile, according to (19), as the harmonic frequency increases, the impedance of the harmonic circuit continuously increases. The ratio of the harmonic current at t=0 to the total output current gradually decreases as the harmonic order increases. This means that higher-frequency harmonics contribute less to the overall output current compared to lower-frequency harmonics. Therefore, the 3rd, 5th, and 7th harmonic orders are considered as the major components influencing the system due to their significant impact.

According to the research conclusions in [27], in order to reduce the turn-on loss of the inverter, it is desirable for the inverter to operate in the ZVS state. Taking the conventional silicon carbide device as an example, when the inverter ZVS condition is met, the minimum instantaneous current required by the inverter is related to the DC input voltage. At the same time, considering that the minimum current required by the inverter to achieve ZVS under different input voltages is different, the subsequent qualitative analysis is only carried out, rather than quantitative current analysis.

The 3-channel ISOP-IPT system is also taken as an example, the parameter data in Table 4 were substituted into the above output current equation for calculation, and the influence of cross coupling on the working state of the ZVS of each channel inverter was verified.

As shown in Fig. 9, under the influence of cross-coupling inductance, as the load resistance increases in a multi-channel ISOP-IPT system, the instantaneous current of the outer channels exceeds 5 A within the range of load variation. However, the instantaneous current of the inverter output in the inner channels decreases continuously as the load resistance increases, approaching 0 A when it exceeds 15 Ω. This indicates an increased risk of the inner channels losing the ZVS operating state. To prevent the increased component losses and failure risks in the inner channels due to inconsistent operating states, it is necessary to compensate for the cross-coupling inductance that affects the fundamental impedance at the output terminals of the inverters in the system. This compensation is essential to eliminate the risk of losing the ZVS operating state caused by cross-coupling inductance.

IV ELIMINATION OF CROSS-INDUCTANCE EFFECTS

According to the analysis in Section III, when cross-coupling inductance exists, the fundamental impedance angle of each channel in the system decreases as the load resistance increases. This means that the instantaneous value of the output

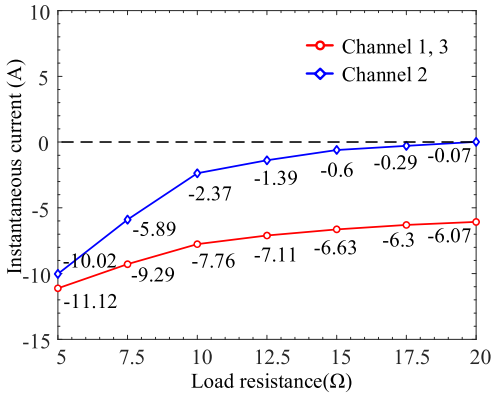

FIGURE 9. Variation trend of the output current of inverters in each channel in a 3-channel ISOP-IPT system under different loads.

current of the inner-channel inverter approaches zero when it turns on, making it prone to losing the ZVS operating state. Besides, the working status of the channels is inconsistent, which increases the fault risk of some channels. Therefore, in this section, the impact of cross-coupling inductance is compensated using a parameter compensation method to achieve equivalent decoupling among all channels in the system and restore the consistency of transmission characteristics.

A. PARAMETER COMPENSATION METHOD TO ELIMINATE THE INFLUENCE OF SAME-SIDE MUTUAL INDUCTANCE

According to the analysis of (13), (14) and (15), only the same side mutual inductance M_a between each channel has an effect on the fundamental impedance angle of the inverter output. Therefore, when compensating for the impact of cross-coupling inductance, it is only necessary to consider eliminating the effects of same-side mutual inductance. Moreover, for the multi-channel system, the relative position between the same-side coils is basically fixed after installation, which means that the same-side mutual inductance between the channels is relatively fixed and does not change with the change of transmission distance [27]. Therefore, after eliminating the same-side mutual inductance, the equivalent decoupling of each channel of the system can be realized.

At the same time, the inconsistent input voltage and output current between channels due to the influence of cross-coupling inductance can be equivalently attributed to the inconsistency caused by transmission inductance. Therefore, subsequent analysis can be performed without considering the effects of cross-coupling inductance. When mutual inductance on the same side of each channel is eliminated ($M_a = 0$), the compensation network parameters of each channel meet the condition of full resonance, and the output impedance of each channel inverter is shown in (22) shown at the bottom of this page. At this time, when not considering the inductive components of the rectifier's equivalent impedance, the equivalent impedance at the output terminal of each inverter in the system is purely resistive.

When the mutual inductance of the same side is eliminated through the compensation element, the equivalent load ratio of the rectifier between the channels is obtained by combining the (11), (15) and (22) as follows:

$$K_i^{\pm} = \frac{R_{eqi}}{R_{eq(i\pm1)}} = \frac{\dot{U}_{in(i\pm1)}}{\dot{U}_{ini}} = \frac{Z_{i\pm1}}{Z_i} \tag{23}$$

According to (23), when the influence of mutual inductance on the same side is eliminated, $K_i^{\pm}$ is independent of the load resistance, which can be obtained by solving the n-element quadratic equations with known system parameters.

In order to eliminate the mutual inductance on the same side of the system, the transmitting coil and the receiving side of each channel are compensated in series respectively. After adding the compensation element, the voltage equation of the transmitting coil branch on the transmitting side of the inner channel (24.1) shown at the bottom of next page and the voltage circuit equation on the receiving side (24.2) shown at the bottom of next page are obtained.

Where the $M_{api(i\pm1)}$ and $M_{asi(i\pm1)}$ is the mutual inductance on the same side, and $M_{bi(i+1)}$ is the cross mutual inductance between different channels.

According to (24.1), in order to eliminate the mutual inductance on the same side of the transmitting side, the compensation impedance element Z_{api_in} should be equal to:

$$Z_{api\_in} = -j\omega\left(M_{api(i+1)}K_{Li}^{+} + M_{api(i-1)}K_{Li}^{-}\right) \tag{25}$$

Similarly, according to (24.2), the compensation impedance element Z_{asi_in} should be equal to:

$$Z_{asi\_in} = -j\omega\left(M_{asi(i+1)}K_{i}^{+} + M_{asi(i-1)}K_{i}^{-}\right) \tag{26}$$

Through the above analysis, it can be seen that the series capacitor is needed as the series compensation element to eliminate the influence of mutual inductance on the same side. The parameter calculation equation of the mutual inductance compensation capacitance of the inner channel is as follows:

$$\begin{cases} C_{api\_in} = \frac{1}{\omega^2\left(M_{api(i+1)}K_{Li}^{+} + M_{api(i-1)}K_{Li}^{-}\right)} \\ C_{asi\_in} = \frac{1}{\omega^2\left(M_{asi(i+1)}K_{i}^{+} + M_{asi(i-1)}K_{i}^{-}\right)} \end{cases} \tag{27}$$

$$\begin{cases} Z_i = L_i\left[C_i\left(\frac{\omega^2\left(M_i + M_bK_{Li}^{\pm}\right)\left(M_i + M_bK_i^{\pm}\right)}{R_{eqi}}\right)\right]^{-1} \cdots (i = 1, n) \\ Z_i = L_i\left[C_i\left(\frac{\omega^2\left[M_i + M_b\left(K_{Li}^{+} + K_{Li}^{-}\right)\right]\left[M_i + M_b\left(K_i^{+} + K_i^{-}\right)\right]}{R_{eqi}}\right)\right]^{-1} \cdots (i \neq 1, n) \end{cases} \tag{22}$$

The equation of mutual inductance compensation capacitance required for the outer channels can be obtained by repeating the above analysis process again:

$$\begin{cases} C_{api\_out} = \dfrac{1}{\omega^2 M_{api(i\pm1)} K_{Li}^{\pm}} \\ C_{asi\_out} = \dfrac{1}{\omega^2 M_{asi(i\pm1)} K_{i}^{\pm}} \end{cases} \tag{28}$$

In order not to change the system topology and not to increase the number of circuit components, the $C_{pi}, C_{si}, C_{api\_in}, C_{asi\_in}$ can be equivalent to a series equivalent capacitor C_{eqpi_in} and C_{eqsi_in}.

According to (27) and (28), the series equivalent capacitance can be obtained as shown in (29).

$$\begin{cases} C_{eqpi\_in} = \dfrac{C_{pi}}{1+C_{pi}\omega^2\left(M_{api(i+1)}K_{Li}^{+}+M_{api(i-1)}K_{Li}^{-}\right)} \\ C_{eqsi\_in} = \dfrac{C_{si}}{1+C_{si}\omega^2\left(M_{asi(i+1)}K_{i}^{+}+M_{asi(i-1)}K_{i}^{-}\right)} \\ C_{eqpi\_out} = \dfrac{C_{pi}}{1+C_{pi}\omega^2 M_{api(i\pm1)}K_{Li}^{\pm}} \\ C_{eqsi\_out} = \dfrac{C_{si}}{1+C_{si}\omega^2 M_{asi(i\pm1)}K_{i}^{\pm}} \end{cases} \tag{29}$$

Combined with the parameters in Table 4, the series equivalent capacitance of the 3-channel ISOP-IPT system is calculated according to (29).

$$C_{eqpi\_in} = 41.490\ \text{nF}, C_{eqsi\_in} = 35.325\ \text{nF}$$

$$C_{eqpi\_out} = 42.871\ \text{nF}, C_{eqsi\_out} = 36.226\ \text{nF}$$

After compensating the mutual inductance on the same side, the fundamental impedance angle changes of the inverter output in each channel of the system are shown in Fig. 10. As can be seen from Fig. 10, after compensation, the fundamental impedance angle at the output terminals of the inverters in each channel is unaffected by changes in the load resistance. The variation trend remains the same as when cross-coupling inductance is not considered, allowing for equivalent presence of inductive components in the equivalent impedance of the rectifier, the fundamental impedance angle of each channel increases with an increase in load resistance.

At the same time, in the load range above 5 Ω, there is an inductive component to maintain the ZVS operation of the inverters. The inconsistent fundamental phase difference between the inner and outer channels in the figure is caused by decoupling among all channels in the system. Due to the presence of cross coupling inductance $M_{bi(i\pm1)}$ between different sides. Meanwhile, the influence of cross coupling inductance between different sides in different channels is shown in Fig. 11. According to (24), the equivalent mutual

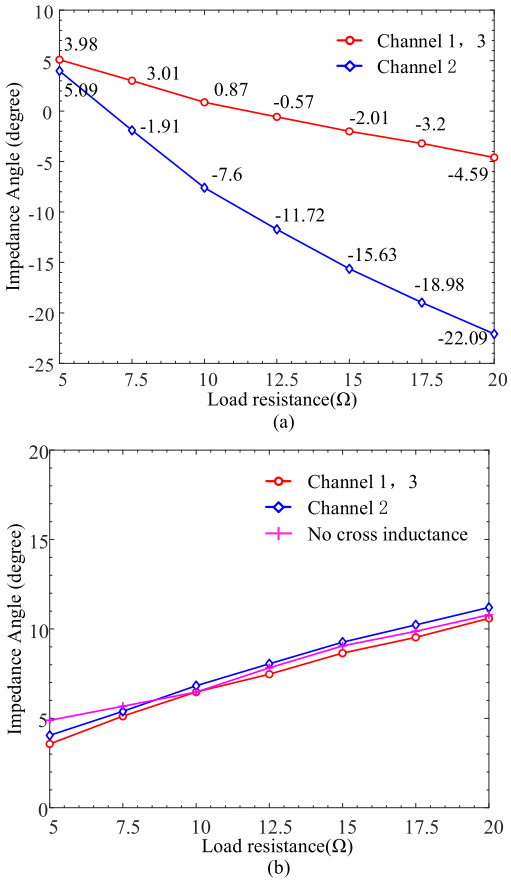

FIGURE 10. The change of fundamental impedance angle of each channel after compensation under different loads (a) before compensation (b) after compensation and without consideration of cross-inductance.

$$\dot{U}_{pi} = \left(Z_{api\_in} + j\omega L_{pi} + \frac{1}{j\omega C_{pi}} + j\omega M_{api(i+1)}K_{Li}^{+} + j\omega M_{api(i-1)}K_{Li}^{-}\right)\dot{I}_{pi} - \left(j\omega M_i \dot{I}_{si} + j\omega M_{bi(i+1)}\dot{I}_{s(i+1)} + j\omega M_{bi(i-1)}\dot{I}_{s(i-1)}\right) \tag{24.1}$$

$$0 = \left(R_{eqi} + j\omega M_{asi(i+1)}K_{i}^{+} + j\omega M_{asi(i-1)}K_{i}^{-} + Z_{asi\_in}\right)\dot{I}_{si} - \left(j\omega M_i \dot{I}_{pi} + j\omega M_{b(i+1)i}\dot{I}_{p(i+1)} + j\omega M_{b(i-1)i}\dot{I}_{p(i-1)}\right) \tag{24.2}$$

$$\begin{cases} M_{eqi} = \sqrt{\left(M_i + M_{bi(i\pm1)}K_{i}^{\pm}\right)\left(M_i + M_{b(i\pm1)i}K_{Li}^{\pm}\right)} \cdots (i = 1, n) \\ M_{eqi} = \sqrt{\left(M_i + M_{bi(i+1)}K_{i}^{+} + M_{bi(i-1)}K_{i}^{-}\right)\left(M_i + M_{b(i+1)i}K_{Li}^{+} + M_{b(i-1)i}K_{Li}^{-}\right)} \cdots (i \neq 1, n) \end{cases} \tag{30}$$

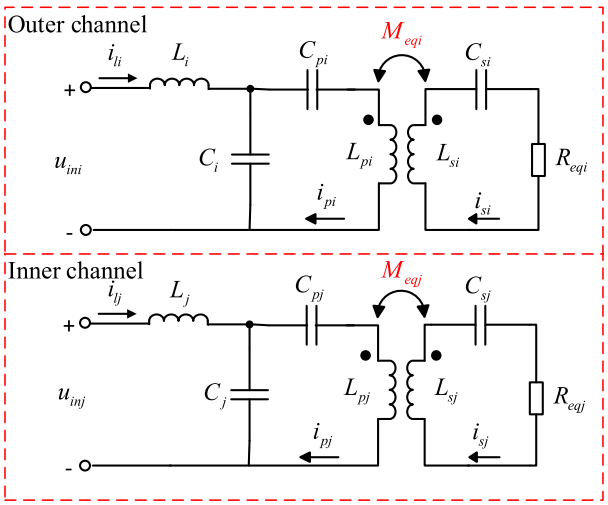

FIGURE 11. The Steady-state circuit diagram of each channel after compensation of mutual inductance on the same side.

inductance formula can be obtained as shown in (30) shown at the bottom of this page.

According to (22), it can be directly equivalent to the inconsistency between transmission mutual inductance, so that the cross-coupling inductance influence is transformed into the inconsistency problem between transmission mutual inductance among channels without considering cross coupling.

To sum up, after eliminating the influence of cross coupling inductance based on parameter compensation method, this section achieves the consistency of working state among channels of multi-channel ISOP-IPT system. The system with cross-coupling can be equivalent to the case without cross-coupling, which is convenient for the subsequent circuit analysis and control research of the system on this basis.

B. PARAMETER DESIGN METHOD OF SYSTEM INPUT VOLTAGE EQUALIZAT-ION

After eliminating the inconsistencies of ISOP-IPT system operation caused by same-side mutual inductance, the remaining influence of cross-inductance will lead to the problem of unbalanced input voltage. To solve this problem, the input voltage can be equalized by adjusting the parameter ratio of transmitting side compensation network between channels. At this time, the equivalent mutual inductance of each channel of the system can be calculated according to (30).

According to (6) and (23), the input voltage ratio between ISOP-IPT system channels after same-side mutual inductance is eliminated is as follows:

$$K_i^{\pm} = \frac{Z_{i\pm1}}{Z_i} = \frac{U_{C(i\pm1)}}{U_{Ci}} = \frac{L_{(i\pm1)}M_{eqi}}{L_i M_{eq(i\pm1)}} \tag{31}$$

Based on (31), the voltage inconsistency caused by cross mutual inductance can be eliminated by adjusting the proportion of series compensation inductors between channels while keeping the resonant state of each channel compensation network unchanged. The adjusted compensation capacitance

TABLE 5. Simulation Parameters of Each Channel in ISOP System

Symbol	Value	Symbol	Value
L_1/μH	15	$C_1/$nF	233.7
L_2/μH	16.873	$C_2/$nF	207.8
L_3/μH	15	$C_3/$nF	233.7
L_{pi}/μH	95	L_{si}/μH	95
$C_{p1}/$nF	42.755	$C_{s1}/$nF	36.144
$C_{p2}/$nF	42.689	$C_{s2}/$nF	35.413
$C_{p3}/$nF	42.755	$C_{s3}/$nF	36.144
M_i/μH	20	M_a/μH	2
M_b/μH	2	f/kHz	85
R_L/Ω	5	$U_{in}/$V	700

values of each channel in the system are substituted into (29), and $K_i^{\pm}$ and $K_{Li}^{\pm}$ are set to 1 to obtain the final equivalent series compensation capacitance.

Taking the compensation parameters in Table 4 as an example, the above analysis is verified based on the 3-channel ISOP-IPT system simulation model. The calculated compensation parameters are shown in Table 5. The system input voltage ratio before compensation is:

$$\frac{U_{C1}}{U_{C2}} = 1.125, \ \frac{U_{C1}}{U_{C3}} = 1$$

The DC input voltage waveform of the system after compensation is shown in Fig. 12. At this time, each channel of the system still has the impedance Angle variation trend as shown in Fig. 10(b), which eliminates the influence of same side-mutual inductance and solves the voltage imbalance caused by cross inductance.

V EXPERIMENTAL VERIFICATION

A. CONSTRUCTION OF 3-CHANNEL ISOP-IPT EXPERIMENTAL SYSTEM

In order to prove the correctness of the above theoretical analysis and parameter compensation, a 3-channel ISOP-IPT system was built, as shown in Fig. 13. The system mainly includes an adjustable DC voltage source, three high-frequency inverter modules, three pairs of transmission coupling coils and LCC-S compensation network components, three uncontrolled rectifier modules and a load resistor. The control part of the system adopts DSP control board, which integrates the FPGA module of 100 MHz operating frequency with TMS320F28335 chip and its basic working module. The square wave generated by the FPGA module acts as the driver signal of the gate driver. To generate a signal that meets the system's operating frequency of 85 kHz, 588 FPGA clocks need to be counted. The MOSFETs model of inverters are APT30SCD120 and the diodes model of rectifiers are C2M0025120D. The transmission coupling coil specification is 650 mm∗650 mm, the transmission distance is 75 mm, and

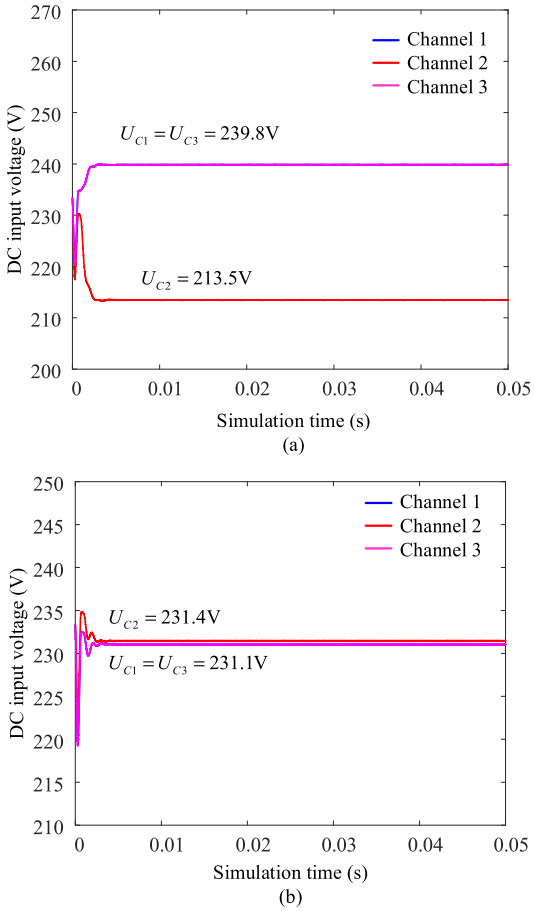

FIGURE 12. System input voltage waveform under the influence of cross-inductance. (a) Before compensation. (b) After compensation.

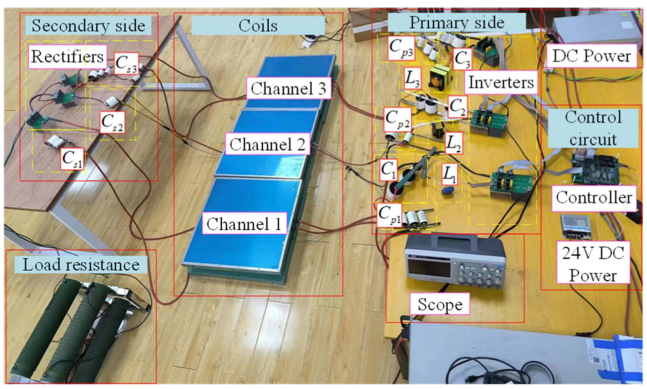

FIGURE 13. Diagram of 3-channel ISOP-IPT experimental system.

the transmitting and receiving coils are closely arranged. System compensation network parameters are shown in Table 6.

B. VERIFICATION OF SYSTEM POWER ENHANCEMENT CAPABILITY

When cross-coupling is not considered, the transmission power of the 3-channel ISOP-IPT system is shown in Fig. 14.

TABLE 6. Experimental Parameters of 3-Channel ISOP-IPT System

Symbol	Value	Symbol	Value
L_1/μH	25.7	C_1/nF	135.9
L_2/μH	19.66	C_2/nF	180.9
L_3/μH	32.5	C_3/nF	108.44
L_{p1}/μH	96.81	C_{p1}/nF	48.74
L_{p2}/μH	94.43	C_{p2}/nF	46.4
L_{p3}/μH	94.58	C_{p3}/nF	56.26
L_{s1}/μH	97.16	C_{s1}/nF	36.11
L_{s2}/μH	96.22	C_{s2}/nF	36.49
L_{s3}/μH	95.98	C_{s3}/nF	35.57
M_1/μH	33.9	M_2/μH	29.75
M_3/μH	32.68	M_{ap12}/μH	2.65
M_{ap23}/μH	2.45	M_{as12}/μH	2.9
M_{as23}/μH	2.42	M_{b12}/μH	1.6
M_{b21}/μH	1.35	M_{b23}/μH	1.95
M_{b32}/μH	1.78	f/kHz	85
R_L/Ω	5~20	U_{in}/V	200

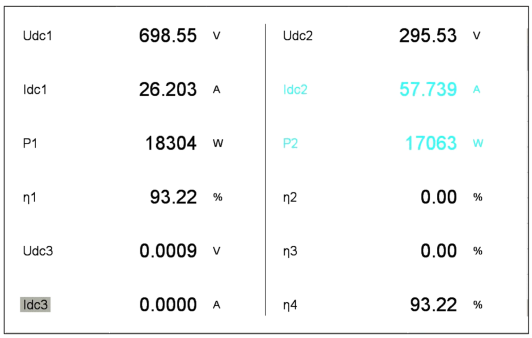

FIGURE 14. Transmission power diagram of a 3-channel ISOP-IPT system.

Limited by the power of the experimental platform, the DC input voltage of the system is 700 V, the input efficiency is 93.22%. The DC input voltage of the three channels of the system is 224 V, 190.4 V, 282.59 V respectively. The theoretical value of input voltage ratio of each channel is$k_{12} = 1.176$, $k_{13} = 0.784$.The actual value of the input voltage ratio of each channel is $k'_{12} = 1.147$, $k'_{13} = 0.76$. The feasibility of constant voltage compensation network is verified.

At this time, the single-channel IPT system is shown in Fig. 15. Keep the DC input current and output voltage the same for single-channel and 3-channel system. When the system transmission power is increased from 5.35 kW in single channel to 17.06 kW in 3-channel, the system input current is 24.59A and 26.2A respectively. This avoids input losses caused by excessive bus current. At the same input voltage and current pressure, the 3-channel ISOP-IPT system achieves a significant increase in transmission power compared to the single-channel system. The enhancement ability is affected

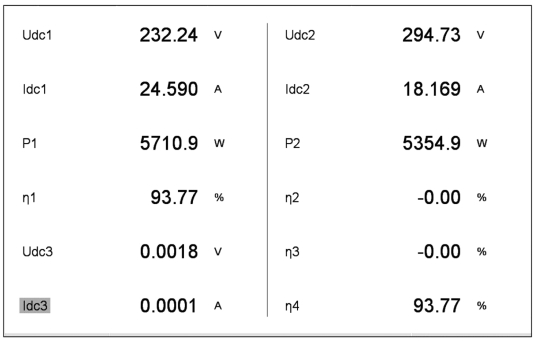

FIGURE 15. Transmission power diagram of a single channel IPT system.

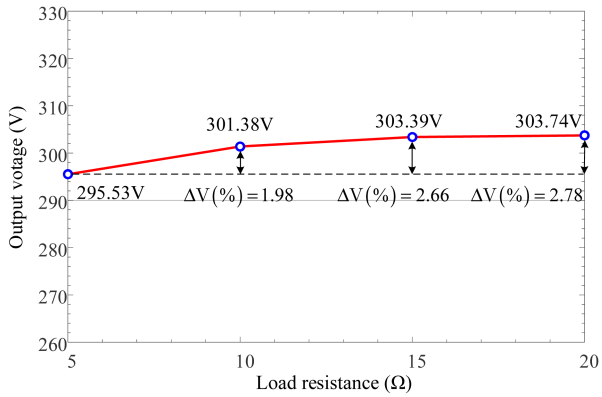

FIGURE 16. output voltage of the system under different loads.

by specific system parameters, but basically conforms to the theoretical analysis in Section II of this paper.

The above experimental results show that the DC input voltage ratio of each channel satisfies (6). The transmission characteristics of ISOP-IPT system are verified. The output voltage of the system under different loads is shown in Fig. 16. The system has a constant voltage output characteristic independent of load.

C. EXPERIMENTAL VERIFICATION OF THE INFLUENCE OF THE TRANSMISSION CHARACTERISTICS OF EACH CHANNEL IN THE PRESENCE OF CROSS-INDUCTANCE

Firstly, the correctness of the theoretical analysis in Section III is verified by experiment. The output fundamental impedance angle of each inverter in 3-channel ISOP-IPT system decreases with the increase of load resistance under the condition of full resonance. At the same time, channel 2, as the inner channel, is affected by the greater mutual inductance on the same side of the two adjacent channels, and the fundamental wave impedance angle decreases more greatly. The instantaneous value of the output current at the moment when the inverter is turned on gradually approaches zero, which makes it highly susceptible to losing the ZVS operation state and affecting the stability of the system. The influence of cross inductance is more obvious in low power condition.

TABLE 7. Compensating Capacitance Parameters for Each Channel

Symbol	Value	Symbol	Value
C_{p1}/nF	47.05	C_{s1}/nF	35.32
C_{p2}/nF	43.37	C_{s2}/nF	32.82
C_{p3}/nF	54.21	C_{s3}/nF	36.04

Therefore, considering the safety of the experiment and the electromagnetic interference caused by the loss of ZVS in the inverter affecting the control signal, the input voltage for the experiment is controlled at 200 V.

The actual measurement parameters of the system are shown in Table 6. The load resistance is selected at four points: 5 Ω, 10 Ω, 15 Ω, and 20 Ω.

The voltage and current waveforms of the inverter output terminals of channels 1 and 3, which are outer channels, under different loads are shown in Fig. 17. At this point, the output current waveforms of the outer channel inverters are generally consistent. With the increase of the load resistance, the instantaneous value of the current at the turn on time of the inverter decreases, but it can still work in the ZVS state with high consistency. However, when cross coupling is considered, the inverter output between the inner and outer channels are inconsistent under different loads.

The inverter output voltage and current waveform of channel 1 and channel 2 is shown in Fig. 18. Found that with the increase of load resistance, the output current of each channel inverter gradually decreases. At the same time, the instantaneous current value at the opening time of the inner channel is gradually close to 0. Starting from a load resistance of 10 Ω, there is a noticeable lag phenomenon in the output voltage and current of inverter channel 2. The operating states of each channel become inconsistent. Moreover, there are oscillations and disturbances in the output voltage, leading to a decrease in system stability.

D. VERIFICATION OF CROSS-MUTUAL INDUCTANCE ELIMINATION METHOD BASED ON PARAMETER COMPENSATION

Eliminating the influence of cross-coupling on the system can remove the coupling state between the channels of the system, so that the system can work in the independent working state of each channel. Finally, the whole multi-channel system is equivalent to multiple single-channel systems working together, simplifying the subsequent analysis process of ISOP-IPT system.

The parameters of the series compensation capacitance of each channel are calculated according to (23), (29) and existing system parameters, as shown in Table 7.

After compensation, the output voltage and current waveform of inverters in each channel of the system are shown in Figs. 19 and 20. At different load resistances, the output of each channel inverter remains consistent, eliminating the impact of same-side mutual inductance in the cross-coupling

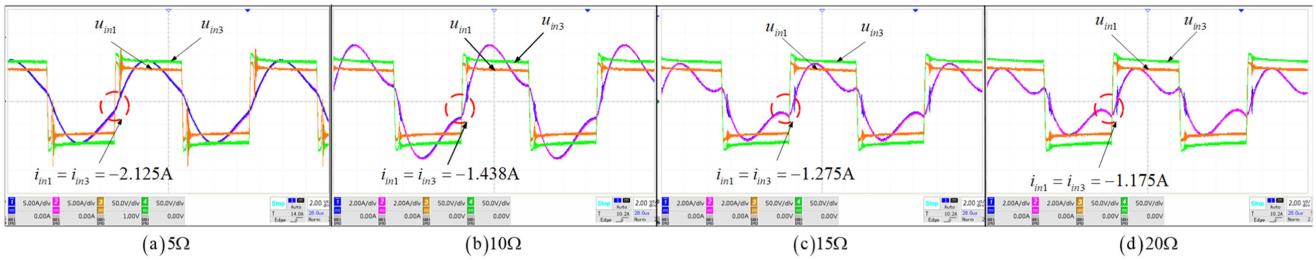

FIGURE 17. Inverter output waveform diagram in the outer channel (channel 1, 3) under different loads.

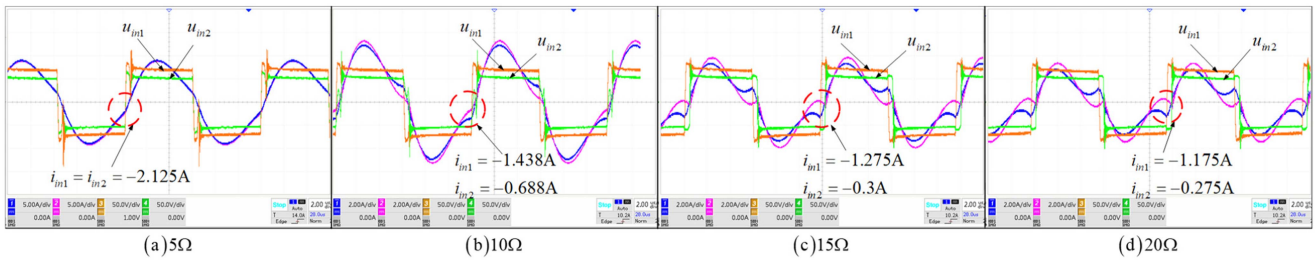

FIGURE 18. Output waveform diagram of inverters in channel 1 and 2 under different loads.

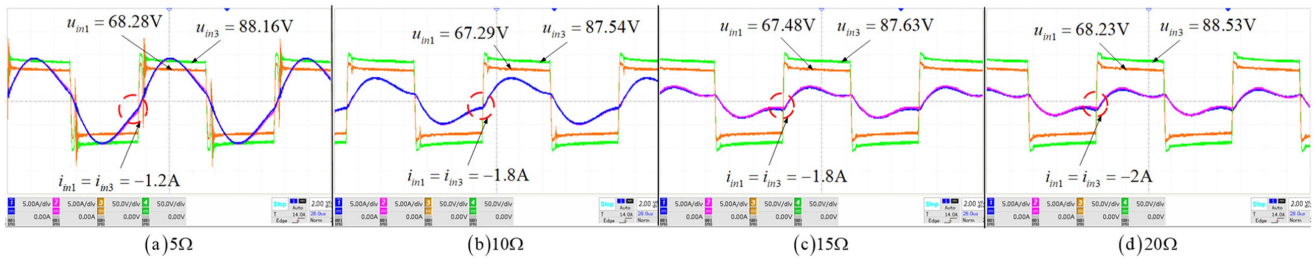

FIGURE 19. Output waveform diagram of inverters in channel 1 and 3 under different loads after compensation.

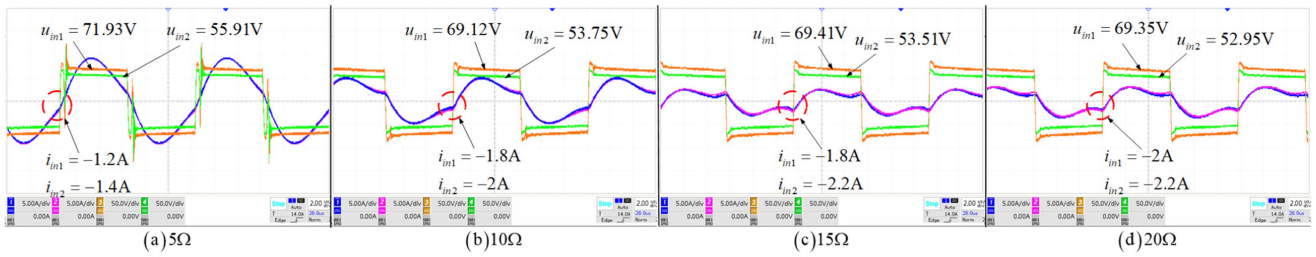

FIGURE 20. Output waveform diagram of inverters in channel 1 and 2 under different loads after compensation.

effect. The transmission characteristics of each channel exhibit a high level of consistency.

Then, the fundamental components of the output voltage and current of the compensated inverter are analyzed, and the output waveform after filtering is shown in Fig. 21. Due to the inconsistency of series compensation inductance and equivalent transmission mutual inductance of each channel, the equivalent impedance of each channel is inconsistent

As a result, the current waveforms in Fig. 21 are not completely consistent. Also, when the load resistance is 5 Ω, the inductive components of the equivalent impedance of each channel in the system are not strong enough. Thus, the inverter outputs lose ZVS, leading to insufficient output stability. With the increase of load resistance, the fundamental impedance angle increases, and the inductance of the equivalent impedance at the output end of the inverter also increases. According

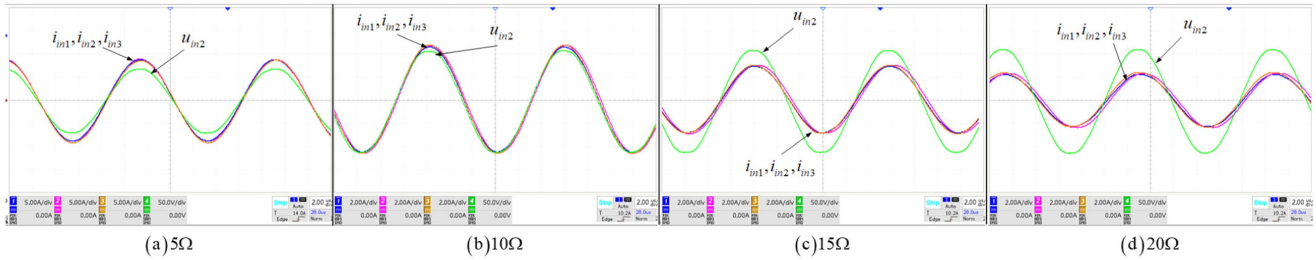

FIGURE 21. Fundamental wave diagram of the output voltage and current of the inverter under different loads after compensation.

TABLE 8. Theoretical and Actual Values of the DC Input Voltage Ratio

Ratio	Theoretical Value	Actual Value
U_{C1}/U_{C2}	1.329	1.288
U_{C1}/U_{C3}	0.776	0.774

to (6) and (30), the theoretical and actual values of the DC input voltage ratio after parameter compensation are shown in the Table 8. The theoretical and actual values are basically consistent. The transmission characteristics of the system are the same as when cross-coupling is not considered. And the equivalent decoupling of each channel is realized by parameter compensation.

VI. CONCLUSION

The multi-channel ISOP-IPT system is analyzed in this paper. It is found that the power transmission capacity of the system can be improved effectively without the use of higher rated power devices. Then, the influence of cross-coupling on the transmission characteristics of the system is analyzed. The research shows that the existence of the same-side mutual inductance will not only lead to the working state inconsistency of each channel, but also increase the analysis complexity of the system's transmission characteristics. Finally, a parameter design method is given to eliminate the working state inconsistency of inverters caused by cross-coupling and realize the equivalent decoupling between each channel.

In the experimental part, a 3-channel experimental system is built. While maintaining the same DC input current and output voltage, the power transmission capacity of the system is increased from 5.35 kW to 17.06 kW, which verifies the power increase capability of the ISOP-IPT system. When cross-coupling exists, the instantaneous current value of the inner channel switching time decreases with the increase of load resistance, and the current difference between channels reaches 0.9A. Experimental findings indicate that without parameter compensation, there is a significant difference in the inverter outputs of the inner and outer channels in the system under different load impedances. After parameter compensation, the instantaneous current value of each channel switch is consistent. And the inductive component of the equivalent input impedance of each channel increases with the increase of load. As a result, the system's channels achieve equivalent decoupling.

REFERENCES

[1] A. Mahesh, B. Chokkalingam, and L. Mihet-Popa, "Inductive wireless power transfer charging for electric vehicles–A review," *IEEE Access*, vol. 9, pp. 137667–137713, 2021.
[2] A. Namadmalan, R. Tavakoli, S. M. Goetz, and Z. Pantic, "Self-aligning capability of IPT pads for high-power wireless EV charging stations," *IEEE Trans. Ind. Appl.*, vol. 58, no. 5, pp. 5593–5601, Sep./Oct. 2022.
[3] M. Haerinia and R. Shadid, "Wireless power transfer approaches for medical implants: A review," *Signals*, vol. 1, no. 2, pp. 209–229, 2020.
[4] K. Qiao, P. Sun, E. Rong, J. Sun, H. Zhou, and X. Wu, "Anti-misalignment and lightweight magnetic coupler with H-shaped receiver structure for AUV wireless power transfer," *IET Power Electron.*, vol. 15, no. 16, pp. 1843–1857, 2022.
[5] E. Rong, P. Sun, K. Qiao, X. Zhang, G. Yang, and X. Wu, "Six-plate and hybrid-dielectric capacitive coupler for underwater wireless power transfer," *IEEE Trans. Power Electron.*, vol. 39, no. 2, pp. 2867–2881, Feb. 2024, doi: 10.1109/TPEL.2023.3334888.
[6] J. Feng, Q. Li, and F. C. Lee, "Omnidirecitional wireless power transfer for portable devices," in *Proc. IEEE Appl. Power Electron. Conf. Expo.*, 2017, pp. 1675–1681.
[7] M. R. Khalid, I. A. Khan, S. Hameed, M. S. J. Asghar, and J.-S. A. Ro, "Comprehensive review on structural topologies, power levels, energy storage systems, and standards for electric vehicle charging stations and their impacts on grid," *IEEE Access*, vol. 9, pp. 128069–128094, 2021.
[8] A. Triviño, J. M. González-González, and J. A. Aguado, "Wireless power transfer technologies applied to electric vehicles: A review," *Energies*, vol. 14, no. 6, 2021, Art. no. 25165.
[9] Y. Li, R. Mai, M. Yang, and Z. He, "Cascaded multi-level inverter based ipt systems for high power applications," *J. Power Electron.*, vol. 15, no. 6, pp. 1508–1516, 2015.
[10] Q. Deng, P. Sun, W. Hu, D. Czarkowski, M. K. Kazimierczuk, and H. Zhou, "Modular parallel multi-inverter system for high-power inductive power transfer," *IEEE Trans. Power Electron.*, vol. 34, no. 10, pp. 9422–9434, Oct. 2019.
[11] Y. Li, R. Mai, L. Lu, T. Lin, Y. Liu, and Z. He, "Analysis and transmitter currents decomposition based control for multiple overlapped transmitters based WPT systems considering cross couplings," *IEEE Trans. Power Electron.*, vol. 33, no. 2, pp. 1829–1842, Feb. 2018.
[12] Y. Liang et al., "Input-series output-series (ISOS) multi-channel ipt system for high-voltage and high-power wireless power transfer," *IEEE J. Emerg. Sel. Topics Power Electron.*, vol. 11, no. 5, pp. 5509–5523, Oct. 2023.
[13] Y. Li et al., "Efficiency analysis and optimization control for input-parallel output-series wireless power transfer systems," *IEEE Trans. Power Electron.*, vol. 35, no. 1, pp. 1074–1085, Jan. 2020.
[14] Q. Deng et al., "Multi-channel inductive power transfer system based on ISOP topology," *J. Power Electron.*, vol. 9, pp. 1–12, 2023.
[15] H. Chen et al., "Modular four-channel 50 kW WPT system with decoupled coil design for fast EV charging," *IEEE Access*, vol. 9, pp. 136083–136093, 2021.
[16] P. Zhao, Y. Jiang, G. Zheng, K. Yue, Y. Liu, and M. Fu, "Heat distribution of IPT receiver with low-voltage and high-current output," in *Proc. IEEE Appl. Power Electron. Conf. Expo.*, 2021, pp. 2565–2570.

[17] Y. Zhang, Y. Wu, W. Pan, Z. Shen, H. Wang, and X. Mao, "A multi-channel wireless charging system with constant-voltage outputs based on LCC-S topology and integrated magnetic design," *Energy Rep.*, vol. 9, pp. 461–468, 2023.
[18] M. Ishihara, K. Fujiki, K. Umetani, and E. Hiraki, "Autonomous system concept of multiple-receiver inductive coupling wireless power transfer for output power stabilization against cross-interference among receivers and resonance frequency tolerance," *IEEE Trans. Ind. Appl.*, vol. 57, no. 4, pp. 3898–3910, Jul./Aug. 2021, doi: 10.1109/TIA.2021.3081071.
[19] L. Cao, J. Bao, K. H. Loo, X. Pan, and R. Zhang, "A hybrid control strategy for dynamic compensation of cross-coupling effect in two-load IPT system," *IET Power Electron.*, vol. 16, pp. 1943–1957, 2023.
[20] M. Fu, T. Zhang, X. Zhu, P. C. -K. Luk, and C. Ma, "Compensation of cross coupling in multiple-receiver wireless power transfer systems," *IEEE Trans. Ind. Informat.*, vol. 12, no. 2, pp. 474–482, Apr. 2016, doi: 10.1109/TII.2016.2516906.
[21] W. Wang, J. Deng, D. Chen, Z. Wang, and S. Wang, "A novel design method of LCC-S compensated inductive power transfer system combining constant current and constant voltage mode via frequency switching," *IEEE Access*, vol. 9, pp. 117244–117256, 2021.
[22] J. Yang, X. Zhang, K. Zhang, X. Cui, C. Jiao, and X. Yang, "Design of LCC-S compensation topology and optimization of misalignment tolerance for inductive power transfer," *IEEE Access*, vol. 8, pp. 191309–191318, 2020.
[23] J. Yang, R. Liu, Q. Tong, X. Yang, Q. Liu, and A. Yao, "Multi-objective optimization of LCC-S-compensated ipt system for improving misalignment tolerance," *Appl. Sci.*, vol. 13, no. 6, 2023, Art. no. 25210.
[24] H. Shen et al., "Mutual inductance and load identification of LCC-S IPT system considering equivalent inductance of rectifier load," *Electronics*, vol. 12, no. 18, 2023, Art. no. 3841.
[25] Y. Jiang, L. Wang, Y. Wang, J. Liu, M. Wu, and G. Ning, "Analysis, design, and implementation of WPT system for EV's battery charging based on optimal operation frequency range," *IEEE Trans. Power Electron.*, vol. 34, no. 7, pp. 6890–6905, Jul. 2019.
[26] S. Li, W. Li, J. Deng, T. D. Nguyen, and C. C. Mi, "A Double-sided LCC compensation network and its tuning method for wireless power transfer," *IEEE Trans. Veh. Technol.*, vol. 64, no. 6, pp. 2261–2273, Jun. 2015.
[27] Y. Liang et al., "Analysis and parameter design for input-series output-series (ISOS) multi-channel inductive power transfer system considering cross coupling," *IEEE J. Emerg. Sel. Topics Power Electron.*, vol. 12, no. 2, pp. 2361–2376, Apr. 2024, doi: 10.1109/JESTPE.2024.3349610.

PAN SUN received the B.S. degree in electrical engineering and automation, and the M.S. degree in electrical engineering from the Naval University of Engineering, Wuhan, China, in 2009 and 2015, respectively. In June 2015, he joined the College of Electrical Engineering, Naval University of Engineering as a Lecturer. He is currently the Director of the Ship Electrical Technology Laboratory and vice Director of the Military Port and Island Power Engineering Military Logistics Research Laboratory. His research interests include wireless power transfer, design, and verification of testability.

LEYU WANG received the B.S. degree in measurement and control Technology and Instrumentation from Jilin University, Changchun, China, in 2022. He is currently working toward the M.S. degree with the Naval University of Engineering, Wuhan, China. His research interests include the design and control of multi-channel wireless power transfer system.

YAN LIANG received the B.S. degree in electrical engineering and automation, and the M.S. degree in electrical engineering from the Beijing Jiaotong University of Engineering, Beijing, China, in 2014 and 2017, respectively. He is currently working toward the Ph.D. degree with the Naval University of Engineering, Wuhan, China. His research interests include robust control method and wireless power transfer.

XUSHENG WU received the B.S., M.S. Tech., and Ph.D. degrees from the College of Electrical and Informational Engineering, Naval University of Engineering, Wuhan, China, in 1996, 1999, and 2004, respectively. He is currently a Professor with the College of Electrical and Informational Engineering, Naval University of Engineering. He is the vice Principal of the Naval University of Engineering and Director of the Military Port and Island Power Engineering Military Logistics Research Laboratory. His research interests include wireless power transfer, electric devices, and power systems on warships.

QIJUN DENG received the B.S and M.Sc. degrees in mechanical engineering, and the Ph.D. degree in computer application technology from Wuhan University, Wuhan, China, in 1999, 2002, and 2005, respectively. In June 2005, he joined the Department of Automation (which now is merged into School of Electrical Engineering and Automation), Wuhan University, where he is currently a Professor. From 2013 to 2014, he was a Visiting Scholar with the New York University Tandon School of Engineering, Brooklyn, NY, USA. His research interests include wireless power transfer, distribution automation, and electrical power informatic.